Different optical absorption edges in AlN bulk crystals grown in *m*- and *c*-orientations

P. Lu,[1] R. Collazo,[1,a)] R. F. Dalmau,[2] G. Durkaya,[3] N. Dietz,[3] and Z. Sitar[1]
[1]*Department of Materials Science and Engineering, North Carolina State University, Raleigh, North Carolina 27695-7919, USA*
[2]*HexaTech, Inc., 991 Aviation Pkwy., Suite 800, Morrisville, North Carolina 27560, USA*
[3]*Department of Physics and Astronomy, Georgia State University, Atlanta, Georgia 30303, USA*

(Received 4 September 2008; accepted 17 September 2008; published online 3 October 2008)

AlN single crystals were grown on *m*-plane $(10\bar{1}0)$ and *c*-plane $(000\bar{1})$ AlN seeds under identical growth conditions. The *m*-plane AlN crystals exhibited substantially lower oxygen incorporation, $\sim 10^{18}$ cm^{-3}, than the *c*-plane crystals, $\sim 10^{19}$ cm^{-3}. By investigating optical transmission spectra, *m*-plane AlN had absorption bands at 4.05 and 4.35 eV, while *c*-plane AlN had an absorption band edge at 4.85 eV. These below bandgap absorption bands strongly correlate with the reported transitions related to Al vacancy-impurity complexes, such as the complex of an Al vacancy and two oxygen atoms, $(V_{Al}-2O_N)^{1-}$ and the complex of an Al vacancy and one oxygen atom, $(V_{Al}-O_N)^{2-}$, becoming the major cause for the poor, below bandgap optical transparency ($\alpha > 200$ cm^{-1}) of these crystals. © *2008 American Institute of Physics*. [DOI: 10.1063/1.2996413]

Owing to its optical[1] and high-temperature electronic properties,[2] single crystal AlN is a promising substrate material for nitride-based optoelectronic devices exploiting the deep ultraviolet (UV) spectral range and for high-frequency electronics. Recent progress in bulk AlN crystal growth has produced AlN crystals grown on SiC templates,[3–5] as well as on native AlN seeds.[6] Seeded crystal growth and expansion has been achieved in polar[7] and nonpolar directions.[8] Limited quantities of (0001) single crystalline AlN wafers are currently available for research[9] and UV light emitting diodes[10] and laser diode structures have been grown on them.[11]

Nevertheless, below bandgap optical absorption bands in the blue/UV range are commonly observed in bulk AlN crystals,[1,12] which are detrimental to the UV transparency and hinder the development of UV optoelectronic devices that depend on susbtrate transparency. Previous studies considered that the absorption bands in the midgap range (3.5–4.5 eV) are caused by the presence of oxygen impurities, aluminum vacancies, and their complexes.[13,14] However, the direct correlation between oxygen impurities and absorption bands still remains unclear. In this letter, by recognizing the difference in impurity incorporation between the AlN bulk crystals grown on *m*-plane $(10\bar{1}0)$ and *c*-plane $(000\bar{1})$ seeds, we compare their corresponding optical transmission spectra, identifying three different absorption edges and the point defects causing them.

To obtain the bulk single crystals, seeded growth of AlN on *m*-plane and *c*-plane $(000\bar{1})$ seeds was performed by physical vapor transport (PVT) using tungsten crucibles in an inductively heated reactor.[15] Sintered AlN powder was held at the bottom of the crucible as the source material, while the seed crystals were attached at the top of the crucible. Single crystal *m*- and *c*-plane AlN seeds were obtained by cutting wafers out of freestanding AlN single crystals. The cuts were made parallel to the desired orientation. Seeds were characterized by x-ray diffraction to confirm the crystallographic orientation and crystal quality. The *m*-plane and *c*-plane $(000\bar{1})$ seeded growths were carried out using identical process conditions. Prior to growth, the reactor chamber was evacuated to a background pressure of 1×10^{-5} Torr, and then filled with N_2 to 500 Torr. During growth, the source temperature was controlled at 2260–2280 °C, while the seed was maintained at 60–80 °C lower temperature. Freestanding crystal boules, 6–7 mm in diameter, 5 mm long, were obtained in about 25 h of growth along either direction, indicating that the crystal growth rate was controlled mainly by the designed thermal profile within the growth crucible rather than by differences due to their crystalline orientation.

In order to study the optical properties of the AlN bulk crystals, *m*- and *c*-plane wafers were cut from the corresponding AlN boules perpendicular to the growth direction and polished on both sides to a final thickness of 175 μm. Figure 1 shows the Raman spectra for the *m*- and *c*-plane AlN wafers. The spectra were taken at room temperature in the backscattering geometry $z(xx)\bar{z}$ using an excitation energy of 2.33 eV. The observed phonon modes in the Raman spectra of *c*- and *m*-plane AlN wafers obey the C_{6v} point group symmetry rules for the corresponding scattering configuration. The E_2(low), E_2(high), and A_1(LO) modes were observed in the *c*-plane wafer. The full width at half maximum (FWHM) of the peak for the E_2(high) mode was 3.9 cm^{-1}. Raman scattering in the $z(xx)\bar{z}$ configuration in an *m*-plane wafer translates into scattering in the $x(yy)\bar{x}$ configuration for a wurtzite structure. The A_1(TO), and E_2(high), and E_2(low) modes were observed in the *m*-plane wafer. The FWHM of the peak for the A_1(TO) mode was 6.4 cm^{-1}. The observed Raman spectra of *c*- and *m*-plane AlN wafers are in agreement with the expected modes for the given crystal orientations.[16]

The impurity incorporation in the *m*- and *c*-plane AlN crystals was characterized by secondary ion mass spectroscopy (SIMS). SIMS depth profiling was performed using a CAMECA IMS-6f with a 50 nA Cs^+ beam over a 180 $\times$ 180 μm^2 area. Three major impurities, silicon, carbon, and

a)Electronic mail: rcollaz@ncsu.edu.

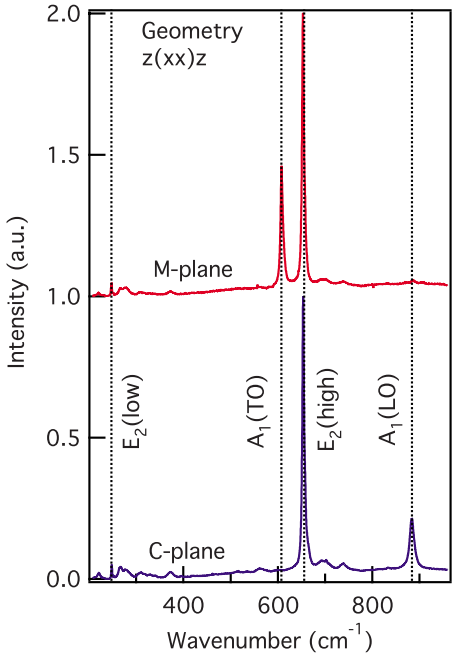

FIG. 1. (Color online) Raman spectra for the *m*- and *c*-plane AlN wafers taken at room temperature in the $z(xx)\bar{z}$ geometry. The dashed lines represent the positions of the different AlN Raman peaks.

oxygen were detected within the AlN crystals, as represented by the calibrated SIMS depth profile shown in Fig. 2. The oxygen concentration in the *c*-plane AlN crystal was 1×10^{19} cm^{-3}, which is consistent with literature reports of AlN bulk crystals grown by the PVT-based methods.[13] In the *m*-plane grown AlN crystal, the detected oxygen concentration was 2×10^{18} cm^{-3}, corresponding to the background level for this measurement; thus, the actual oxygen concentration is at or below this concentration. Since the *m*- and *c*-plane AlN crystals were grown using the same growth reactor, source materials, and process conditions, the difference in the oxygen incorporation is related to the difference in chemical reactivity and kinetics on the two different surface orientations. This translates into a different behavior for the incorporation of intentional and unintentional impurities and generation of other point defects as a response to a given process supersaturation for each type of crystallographic planes. An example of this point has been observed in GaN, where the calculated adsorption energy for oxygen under low surface coverage is estimated to be around 1 eV/atom lower

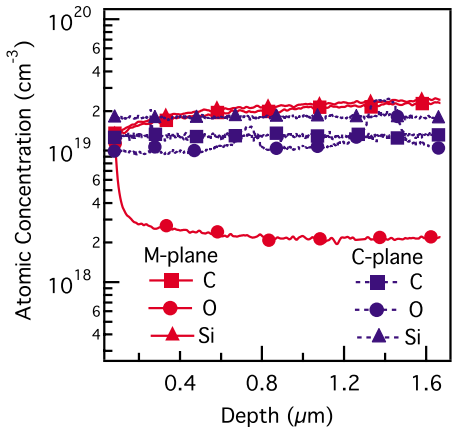

FIG. 2. (Color online) SIMS depth profile of *c*-plane and *m*-plane AlN for oxygen, carbon, and silicon.

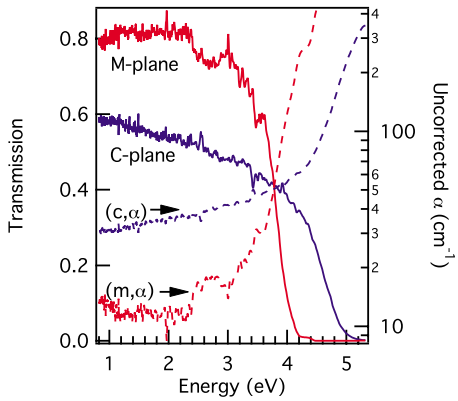

FIG. 3. (Color online) Optical transmission spectra and uncorrected absorption coefficient α for the *m*-plane and *c*-plane grown AlN crystals recorded between 0.8 and 5.3 eV.

for a $(000\bar{1})$ surface than that for a (0001) surface for the corresponding expected reconstructions during growth.[17] Differences in the impurity incorporation between different facets are expected to occur during growth of bulk AlN, although they have not been directly measured.[12] In addition, orientation dependent effects have been observed in impurity dopant incorporation of III-V semiconductors grown by metal-organic vapor phase epitaxy.[18] The *m*- and *c*-plane grown AlN exhibited the same amount of silicon, 2×10^{19} cm^{-3}, indicating that the formation energy of the silicon impurity is either similar on *m*- and *c*-planes of AlN, or it is very low, so that the silicon incorporation is controlled by mass transport and not by different surface chemistries. The *m*-plane AlN had twice the amount of carbon $(2\times10^{19}$ cm$^{-3})$ as compared to the *c*-plane AlN $(1\times10^{19}$ cm$^{-3})$.

Optical transmission measurements of the crystals were recorded between 0.8 and 5.3 eV (1550 and 235 nm), allowing the investigation of the impurity-related transition bands in the near infrared, visible, and UV range, as shown in Fig. 3. The *m*-plane AlN has a transmission cutoff between 4.0 and 4.1 eV, whereas the *c*-plane AlN has a transmission cutoff between 4.8 and 4.9 eV. Both wafers have a significant reduction in the transmission below the bandgap (6.1 eV). Figure 3 also shows the uncorrected (spectral reflectance data is not available) absorption coefficient α for the two different wafers. It is important to establish that the expected absorption coefficient at the AlN fundamental absorption edge is on the order of 10^5 cm^{-1} or several orders of magnitude higher than the absorption coefficients from Fig. 3. Assuming a transition between an acceptorlike defect level and the empty conduction band, the absorption coefficient should be proportional to the product of the defect density, N_s, and the conduction band density of states at the transition energy, $\alpha\hbar\omega\propto N_S\sqrt{\hbar\omega-(\varepsilon_G-\Delta\varepsilon_S)}$, where ε_G is the energy band gap and $\Delta\varepsilon_S$ is the acceptor ionization energy. Figure 4 shows a plot of the square of the product of the absorption coefficient and the photon energy as a function of photon energy in order to determine the energy of different absorption edges for both *m*- and *c*-plane AlN.[19] Straight lines can be fitted through the measured data, and their intersections with the abscissa yield the energy position of the absorption band edges. In *c*-plane AlN, one sharp absorption band edge is observed at 4.85 eV, while in *m*-plane AlN, two absorption band edges are observed at 4.05 and 4.35 eV.

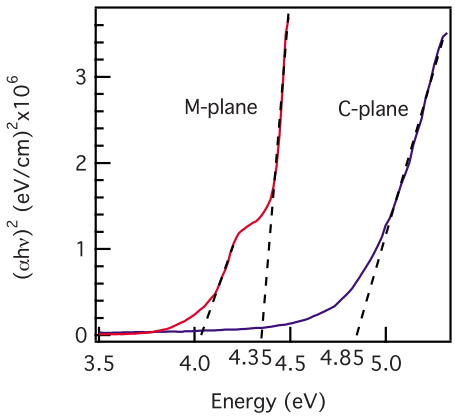

FIG. 4. (Color online) The square of the product of the absorption coefficient and the quantum energy as a function of the quantum energy for *m*-plane and *c*-plane AlN. The energy values represent the position of the intersection of the straight line with the abscissa.

Absorption bands below the bandgap in GaN, AlGaN, and AlN have been attributed to impurity electronic transitions related to the presence of deep acceptors.[20–22] In AlN, the deep acceptors can be an isolated Al vacancy with three negative charges $(V_{Al})^{3-}$ or the Al vacancy complex with two negative charges or one negative charge $(V_{Al}$ complex$)^{2-}$ and $(V_{Al}$ complex$)^{1-}$. The absorption band edge at 4.85 eV closely matches the energy (4.7 eV) of the transition associated with the complex of an Al vacancy and two oxygen atoms $(V_{Al}-2O_N)^{1-}$, and the shallow donor or conduction band.[22] Similarly, the absorption band at 4.05 eV is consistent with the transition (4.0 eV) associated with the complex of an Al vacancy and one oxygen atom $(V_{Al}-O_N)^{2-}$, and the shallow donor or conduction band.[20,21] In addition, the calculated difference in binding energy between $(V_{Al}-2O_N)^{1-}$ and $(V_{Al}-O_N)^{2-}$ is about 0.7 eV, which agrees well with our experimental result of 0.8 eV. Therefore, in *c*-plane AlN, in the presence of a larger amount of oxygen, 1×10^{19} cm^{-3}, the stable deep acceptor defect is the complex $(V_{Al}-2O_N)^{1-}$, while in *m*-plane AlN, where the oxygen concentration is much lower, 2×10^{18} cm^{-3}, one of the stable deep acceptor defects is the complex $(V_{Al}-O_N)^{2-}$. Moreover, in *m*-plane AlN, another absorption band edge is observed at 4.35 eV that is clearly not related to the pure Al vacancy $(V_{Al})^{3-}$, which has a much lower transition energy of 3.4 eV.[20,21] The observed absorption band is probably caused by the complex of excess $(V_{Al})^{3-}$ with some other impurity. Since the crystals contain a fair amount of Si, one could suspect a $(V_{Al}-Si_{Al})^{2-}$ complex, however, this would imply interaction between second nearest neighbors, with a corresponding small binding energy. A luminescence peak corresponding to a transition at 4.4 eV has been observed for carbon doped AlN thin films, suggesting that this transition is due to carbon related defects.[23]

In summary, we have investigated the optical transmission of *m*- and *c*-plane AlN single crystals and related the observed absorption band edges to specific point defects. At the reported particular process conditions, *m*-plane AlN exhibited a lower oxygen concentration, 10^{18} cm^{-3}, than *c*-plane AlN, 10^{19} cm^{-3}. However, both orientations incorporated a similar concentration of Si impurities, 10^{19} cm^{-3}. *m*-plane and *c*-plane AlN crystals showed different absorption band edges below bandgap, which are related to the oxygen concentration in the crystals. The energies of the absorption bands, 4.05 eV in *m*-plane and 4.85 eV in *c*-plane AlN, coincide with the energy of the transitions already identified with complexes of Al vacancies and oxygen $(V_{Al}-O_N)^{2-}$ and $(V_{Al}-2O_N)^{1-}$, respectively. In addition, an unidentified absorption band at 4.35 eV in *m*-plane AlN remains unidentified and is likely caused by a complex of Al vacancy and an impurity other than silicon.

[1] M. Strassburg, J. Senawiratne, N. Dietz, U. Haboeck, A. Hoffmann, V. Noveski, R. Dalmau, R. Schlesser, and Z. Sitar, J. Appl. Phys. **96**, 5870 (2004).
[2] M. Neuburger, A. Aleksov, R. Schlesser, E. Kohn, and Z. Sitar, Electron. Lett. **43**, 592 (2007).
[3] C. M. Balkas, Z. Sitar, T. Zheleva, L. Bergman, R. Nemanich, and R. F. Davis, J. Cryst. Growth **179**, 363 (1997).
[4] P. Lu, J. H. Edgar, C. Cao, K. Hohn, R. Dalmau, R. Schlesser, and Z. Sitar, J. Cryst. Growth **310**, 2464 (2008).
[5] B. M. Epelbaum, M. Bickermann, and A. Winnacker, J. Cryst. Growth **275**, 479 (2005).
[6] R. Schlesser, R. Dalmau, and Z. Sitar, J. Cryst. Growth **241**, 416 (2002).
[7] Z. G. Herro, D. Zhuang, R. Schlesser, R. Collazo, and Z. Sitar, J. Cryst. Growth **286**, 205 (2006).
[8] D. Zhuang, Z. G. Herro, R. Schlesser, and Z. Sitar, J. Cryst. Growth **287**, 372 (2006).
[9] S. B. Shujman, L. J. Schowalter, R. T. Bondokov, K. E. Morgan, W. Liu, J. A. Smart, and T. Bettles, J. Cryst. Growth **310**, 887 (2008).
[10] Z. Ren, Q. Sun, S.-Y. Kwon, J. Han, K. Davitt, Y. K. Song, A. V. Nurmikko, H.-K. Cho, W. Liu, J. A. Smart, and L. J. Schowalter, Appl. Phys. Lett. **91**, 051116 (2007).
[11] M. Kneissl, Z. Yang, M. Teepe, C. Knollenberg, O. Schmidt, P. Kiesel, N. M. Johnson, S. Schujman, and L. J. Schowalter, J. Appl. Phys. **101**, 123103 (2007).
[12] M. Bickermann, P. Heimann, and B. M. Epelbaum, Phys. Status Solidi C **3**, 1902 (2006).
[13] G. A. Slack, L. J. Schowalter, D. Morelli, and J. A. Freitas, Jr., J. Cryst. Growth **246**, 287 (2002).
[14] M. Bickermann, B. M. Epelbaum, and A. Winnacker, J. Cryst. Growth **269**, 432 (2004).
[15] V. Noveski, R. Schlesser, S. Mahajan, S. Beaudoin, and Z. Sitar, J. Cryst. Growth **264**, 369 (2004).
[16] M. Bickermann, B. M. Epelbaum, P. Heimann, Z. G. Herro, and A. Winnacker, Appl. Phys. Lett. **86**, 131904 (2005).
[17] T. K. Zywietz, J. Neugebauer, and M. Scheffler, Appl. Phys. Lett. **74**, 1695 (1999).
[18] R. Bhat, C. Caneau, C. E. Zah, M. A. Koza, W. A. Bonner, D. M. Hwang, S. A. Schwarz, S. G. Menocal, and F. G. Favire, J. Cryst. Growth **107**, 772 (1991).
[19] K. Seeger, *Semiconductor Physics*, 7th ed. (Springer, New York, 1999), p. 331.
[20] T. Mattila and R. M. Nieminen, Phys. Rev. B **55**, 9571 (1997).
[21] K. B. Nam, M. L. Nakarmi, J. Y. Lin, and H. X. Jiang, Appl. Phys. Lett. **86**, 222108 (2005).
[22] N. Nepal, M. L. Nakarmi, J. Y. Lin, and H. X. Jiang, Appl. Phys. Lett. **89**, 092107 (2006).
[23] X. Tang, F. Hossain, K. Wongchotigul, and M. G. Spencer, Appl. Phys. Lett. **72**, 1501 (1998).